International Journal of Heat and Mass Transfer 52 (2009) 5072–5080

Contents lists available at ScienceDirect

International Journal of Heat and Mass Transfer

journal homepage: www.elsevier.com/locate/ijhmt

On Taylor dispersion effects for transient solutions in geothermal heating systems

Alexandra Ortan [a,1], Vincent Quenneville-Bélair [a,1], B.S. Tilley [b,*], J. Townsend [b]

[a] Department of Mathematics and Statistics, McGill University, Montréal, Que., Canada
[b] Franklin W. Olin College of Engineering, 1000 Olin Way, Needham, MA 02492, USA

ARTICLE INFO

Article history:
Received 10 May 2008
Received in revised form 20 April 2009
Available online 17 June 2009

Keywords:
Geothermal heating systems
Similarity solutions
Taylor dispersion
Ground coupled heat pump

ABSTRACT

Residential geothermal heating systems have been developed over the past few decades as an alternative to fossil-fuel based heating. Through mathematical modeling the relationship between the operating parameters of the heat pump and the piping length of the geothermal system, which is directly correlated to the cost of the system is investigated. The effect of Taylor dispersion of heat in the fluid which is not yet addressed in the literature with respect to geothermal systems is included. A model of a simple configuration of a single pipe surrounded concentrically by grout and then by soil is considered, where the soil region has a constant ambient temperature. The conduction between the two regions is modeled with a classical thermal resistance. Taylor dispersion effects are significant at higher Peclet numbers associated with this system, and Taylor dispersion in the fluid and thermostat frequency dictate the minimum tubing length needed for successful operation in an insulated subsystem. We consider both steady state and transient (cyclic operation) analyses and find that the axial dispersion increases linearly in the cycle rate for large flow rates. We find that the estimated tubing length for complete energy transport is increased when Taylor dispersion is included, but that this effect can be mitigated with an appropriate choice of the borehole radius.

1. Introduction

Although the promise of environmentally friendly, low-cost energy harnessing for heating and cooling of residential properties has been known for nearly 30 years, the adoption of the technology in the United States has been slow. These geothermal systems, also known as ground-coupled heat pumps, consist of a field of vertical boreholes in the ground with pipes carrying a heat transfer fluid into the earth to gain access to the stable year-round temperatures underground. The fluid is pumped back to the residential unit to be used for heating or cooling depending on the season. A significant portion of the cost for ground-coupled heat pump systems is in the installation of the large networks of piping to harness the geothermal energy. These installation costs are currently cost-prohibitive, with a typical return-time on investment on the order of 8–10 years. One means to improve the economic competitiveness of these systems is to reduce the installation footprint. Our focus in this research program is to develop mathematical models to quantify how the length of the piping is related to the operational parameters of the system. The model developed in this work includes both the effect of cycling (turning the fluid flow on or off in response to the heating or cooling load of the residence) and the effect of axial heat transport, by means of advection and Taylor dispersion, in the pipes.

The main design criteria for these heating systems is the effective power that can be obtained from the fluid heated as it flows through the tubing.[2] The power rating of these systems can be estimated by determining the change in rate of thermal energy of the fluid entering the system from the residence and leaving the system

$$\text{Power} = \rho_w c_w U^* A_p \Delta T,$$

where ρ_w is the density of the fluid, c_w is the specific heat of the fluid, U^* is the characteristic fluid velocity, A_p is the pipe's cross-sectional area, and ΔT is the temperature change. For a given fluid, such as water or ethylene glycol, flow rate and power rating requirement, the required length of pipe needed for the system to function properly is determined from the unknown temperature variation in the axial direction. However, the temperature profile in the fluid is necessarily coupled to the thermal behavior in the soil from which the energy is transferred. In order to fully understand how these systems work, a requirement for design optimization, the temperature profile in both the soil and the fluid need to be solved simultaneously. This is a difficult modeling task, so it is no surprise that some simplifications in the modeling have been attempted in order to understand different aspects of the system.

* Corresponding author.
E-mail address: tilley@olin.edu (B.S. Tilley).
[1] Present address: Department of Mathematics, 127 Vincent Hall, 206 Church St. S.E., University of Minnesota, Minneapolis, MN 55455, USA.

[2] We focus in this work on closed-loop systems.

0017-9310/$ - see front matter © 2009 Elsevier Ltd. All rights reserved.
doi:10.1016/j.ijheatmasstransfer.2009.05.010

Nomenclature

D	dimensionless axial diffusion coefficient
H	dimensionless heat transfer coefficient
L	dimensional characteristic axial length
Nu	scaled Nusselt number, $L^2h/(ak_g)$
P	period of thermostat oscillation (on and off cycles)
Pe	Peclet number, U^*a/α_w
R	radial extent of grout region
T	temperature
U	characteristic axial fluid velocity
a	tubing radius
c	specific heat (J/kg K)
h	heat transfer coefficient
k	thermal conductivity
ℓ	dimensionless axial characteristic length scale
r	radial coordinate
t	time
u	axial fluid velocity
x	axial coordinate
v	thermal front velocity
y	moving frame of reference, $x - vPet$

Greek symbols

α	thermal diffusivity
δ	relative temporal period of oscillation compared to characteristic time-scale
ϵ	aspect ratio, a/L
κ	wavenumber of axial temperature profile
η	dimensionless thermostat cycle rate
ρ	density
σ	spatial exponential growth rate (steady-state solutions)
τ	slow-time, ϵt
θ	dominant grout temperature
$\bar{\theta}$	correction to radial average temperature
ξ	similarity variable, $y/2\sqrt{Dt}$

Subscripts

F	Fourier-law diffusion
T_w	Taylor dispersion effect from water
T_g	Taylor dispersion effect from grout layer
$0, 1, \ldots$	correction of quantity to $O(\epsilon^{0,1,\cdots})$
a	ambient
eff	effective quantity (time-averaged)
g	grout quantity
i	inlet
r	$\partial/\partial r$
s	steady
t	$\partial/\partial t$
u	unsteady
w	water quantity
x	$\partial/\partial x$
τ	$\partial/\partial \tau$

Superscripts

$*$	dimensional quantity
(1)	water quantity
(2)	grout quantity

Analytical approaches to these systems have focused on the thermal behavior of the soil in the cross-section, with the assumption that the temperature profile in the fluid is known. The simplest model used is an adaption of the Kelvin line-source model [1]. This model assumes that a radial heat flux is known from the tubing which is proportional to the temperature difference between the fluid temperature and the soil temperature. To model axial heat transport, the cylinder source model has been applied [2] (a brief and clear review of this models is presented in [3]). This model couples the heat flow between cross-sectional planes of the line-source model with a prescribed thermal resistance [4–6]. Further, a radial thermal resistance is used to decouple the local thermal behavior from the far-field behavior. All of these attempts have not investigated how the advective heat transport in the fluid affects the axial heat flow in the soil in a direct, physically fundamental way. A fundamental approach does not rely on a phenomenologically-based choice for an axial thermal resistance, which then must be modified with a new series of experiments for each new system.

There has been recent interest [3] in developing transient models that can provide better analyses of the short time behavior of the ground heat exchanger (GHE). Dobson [7] showed that cycling the flow (with an on-time on the order of minutes) can improve the efficiency of the system. The development of better transient models will enable better simulation of geothermal systems and improve the optimization of geothermal designs. We are interested in finding a mathematical description, based on the fundamental equations of heat transfer in continuous media, of the near and far-field behavior of the system in order to optimize their design. In this work, we consider the local behavior near the tubing, and include the effect of Taylor dispersion of heat in the tubing and the grout for the simple case of a single pipe within a borehole. Although we assume knowledge of the far-field temperature profile in this work, a subsequent paper in preparation addresses how this local temperature profile is coupled to the far-field distribution over long times.

In order to better understand the dominant mechanisms of the local system, we note that there are two time-scales of interest. The first corresponds to the thermal transport time due to conduction for heat to diffuse through soil, which is on the order of hours. The second time scale is the typical cycle time needed to maintain a residence at a prescribed temperature, which is on the order of minutes. These time scales can be represented mathematically by

$$\text{conduction time} = \frac{a^2}{\alpha_g}, \quad \text{cycle time} = \frac{a}{U^*},$$

where a is the radius of the pipe and α_g is the thermal diffusivity of the grout. The ratio of these time-scales

$$\frac{\text{cycle time}}{\text{conduction time}} = \frac{a\alpha_g}{a^2U^*} = \frac{\alpha}{Pe} \ll 1,$$

where $\alpha = \alpha_g/\alpha_w$ is the ratio of the thermal diffusivities of the grout to the water and $Pe = aU^*/\alpha_w$ is the Peclet number of the fluid flow. Since $\alpha = O(1)$, this suggests that we are interested in the case for large Peclet numbers.

There is a classical result from solutal diffusion in laminar fluid flows found by Taylor [8,9], in which he found an effective diffusion coefficient for the concentration C in a solvent

$$\frac{\partial C}{\partial t} = \left[1 + \frac{Pe^2}{192}\right]\frac{\partial^2 C}{\partial y^2},$$

where time t is on the diffusive time-scale and y is a frame of reference moving with the average fluid velocity. The first term in the effective diffusion coefficient represents Fickian diffusion, whose relative importance decreases with increasing Peclet number. The second term, however, grows quadratically with increasing Peclet number, and this term is called Taylor dispersion. Further, Aris

[10], through an analysis of the concentration distribution, demonstrated that Taylor's analysis is valid for all Peclet numbers, that is, beyond the transition from laminar to turbulent flow. The distribution of solute tends to a normal distribution, whose variance is described by the diffusion coefficient above, and other moments are shown to be negligible in comparison. The analogous effect in geothermal heating has not yet been addressed, and we focus on its implications in our work.

In Section 2, we derive the effective heat transfer equations for a simple cycling problem of a single pipe of fluid, surrounded by a grout with different thermal behaviors in the local and far-field regions. The thermal conductivity between these regions is assumed to be small compared to the times of interest here (1–2 weeks). In Section 3, we summarize how the characteristic length scale of the axial temperature dependence varies with the material properties of the system and the Peclet number. Similarity solutions are found for the steady flow problem and effective temperature equations are found for the unsteady problem. We note that the minimum length needed of tubing for an effective system depends linearly on the cycle rate of the thermostat used in the residence. We state our conclusions in Section 4, and make recommendations based on this model.

2. Problem description

Consider a pipe of radius a which is encircled concentrically by a ring of grout, with an outer radius of R^* as shown in Fig. 1(a). A heat-exchanging fluid, such as water, flows through the pipe from the inlet at $x^* = 0$ with a prescribed inlet temperature T_i. The length of this system is long compared to the pipe radius, and we assume that changes in temperature profile in the liquid vary on some length scale $L \gg a$. This length scale is characterized by an appreciable length such that the heat flux q_{in} is comparable to the power demands of the residence. A cartoon is shown in Fig. 1(b). Surrounding this system is soil, whose ambient temperature T_a is assumed to be constant over the short time-scales under consideration. The main function of residential geothermal heating systems is to leverage the difference between the inlet fluid temperature to the ambient soil temperature in order to perform the heating or cooling of the residence. For simplicity, we assume that the fluid flow in the pipe is a laminar Poiseuille flow of the form

$$u^*(r^*) = \begin{cases} U^*\left[1 - \left(\frac{r^*}{a}\right)^2\right] & \text{“on”}, \\ 0 & \text{“off”}, \end{cases}$$

where U^* is the characteristic fluid flow velocity scale. “on” refers to that time when the pump is running, as commanded by the residence thermostat.

The energy equation within the fluid, assuming all dependence in the azimuthal direction is ignored,

$$T^{(1)}_{t^*} + u^*(r^*)T^{(1)}_{x^*} = \alpha_w\left\{\frac{1}{r^*}\left(r^*T^{(1)}_{r^*}\right)_{r^*} + T^{(1)}_{x^*x^*}\right\}, \quad 0 < r^* < a, \tag{1}$$

where α_w is the thermal diffusivity of the water. In the grout layer, the heat equation is given by

$$T^{(2)}_{t^*} = \alpha_g\left\{\frac{1}{r^*}\left(r^*T^{(2)}_{r^*}\right)_{r^*} + T^{(2)}_{x^*x^*}\right\}, \quad a < r^* < R^*, \tag{2}$$

where α_g is the thermal diffusivity of the grout (see Table 1).

In the radial direction, we assume that no normal flux occurs along the centerline $r^* = 0$, that there is perfect thermal contact along $r^* = a$, and that the normal heat-flux along the grout-soil boundary is balanced by Newton's law of cooling

$$r^*\frac{\partial T^{(1)}}{\partial r^*} \to 0, \quad r^* \to 0, \tag{3}$$

$$T^{(1)} = T^{(2)}, \quad r^* = a, \tag{4}$$

$$k_w\frac{\partial T^{(1)}}{\partial r^*} = k_g\frac{\partial T^{(2)}}{\partial r^*}, \quad r^* = a, \tag{5}$$

$$-k_g\frac{\partial T^{(2)}}{\partial r^*} = h(T^{(2)} - T_a), \quad r^* = R^*, \tag{6}$$

where k_w is the thermal conductivity of the water, k_g is the thermal conductivity of the grout, and h is the heat transfer coefficient between the grout and soil regions. Eq. (6) models the relatively slow rate of heat transport within the soil. We assume the heat transfer between these two regions to be small, but nonzero. The assumption that the soil temperature does not vary in time or in space from its ambient temperature is an idealization over the short time-scales of interest (days), but our interest here is how the operating parameters determine the length required to transfer the required heat to the fluid from the soil. From [11], the heat transfer between these two regions could provide a length scale of interest.

We scale the radial coordinate on the pipe radius a, the axial direction on the characteristic length L, time on the diffusive time scale, and temperature on the temperature difference $\Delta T = T_i - T_a$. Using T_a as a reference temperature within the soil layer and the water, these scales are written as

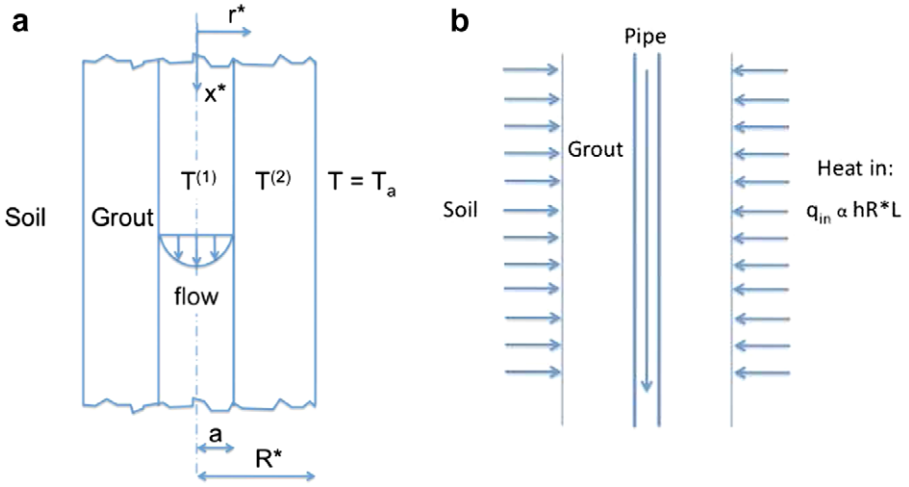

Fig. 1. (a) Problem configuration. (b) Heat exchanger balance: length scale L depends on the rate of heat transport within the soil h.

Table 1
Characteristic dimensional quantities residential geothermal heat pump systems, and the corresponding range for dimensionless parameters.

Dimensional quantities		Dimensionless quantities	
Fluid velocity (m/s)	0.3–5	Reynolds number	3000–100,000
Fluid thermal conductivity (W/m K)	0.6		
Fluid thermal diffusivity (m^2/s)	1.44×10^{-7}	*Pe*	20,000–700,000
Grout thermal conductivity (W/m K)	5.19		
Grout thermal diffusivity (m^2/s)	2.91×10^{-6}		
Grout-soil heat transfer coefficient (W/m^2 K)	10^{-7}	ah/k_g	10^{-10}
Pipe radius (m)	0.01–0.02		
Borehole radius (m)	0.05–0.1	*R*	5
Ambient soil temperature (°C)	10–16		

$$[x^*]=L,\ \ [r^*]=[R^*]=a,\ \ [t^*]=La/\alpha_w,\ \ \frac{T^{(i)}-T_a}{T_i-T_a}\to T^{(i)},\quad i=1,2, \tag{7}$$

and the energy equations (1) and (2), along with the radial boundary conditions, become

$$\epsilon\left\{T_t^{(1)}+Pe(1-r^2)T_x^{(1)}\right\}=\frac{1}{r}\left(rT_r^{(1)}\right)_r+\epsilon^2T_{xx}^{(1)},\ \ 0<r<1\ \text{“on”}, \tag{8}$$

$$\epsilon\left\{T_t^{(1)}\right\}=\frac{1}{r}\left(rT_r^{(1)}\right)_r+\epsilon^2T_{xx}^{(1)},\ \ 0<r<1\ \text{“off”}, \tag{9}$$

$$\epsilon T_t^{(2)}=\alpha\left\{\frac{1}{r}\left(rT_r^{(2)}\right)_r+\epsilon^2T_{xx}^{(2)}\right\},\ \ 1<r<R, \tag{10}$$

$$r\frac{\partial T^{(1)}}{\partial r}\to0,\ \ r\to0, \tag{11}$$

$$T^{(1)}=T^{(2)},\ \ r=1, \tag{12}$$

$$\frac{\partial T^{(1)}}{\partial r}=k\frac{\partial T^{(2)}}{\partial r},\ \ r=1, \tag{13}$$

$$\frac{\partial T^{(2)}}{\partial r}=-\epsilon^2NuT^{(2)},\ \ r=R, \tag{14}$$

where $\epsilon=a/L\ll1$ is the aspect ratio of the pipe, $Pe=U_oa/\alpha_w$ is the Peclet number of the fluid, $\alpha=\alpha_g/\alpha_w$ is the thermal diffusivity ratio, and $k=k_g/k_w$ is the thermal conductivity ratio. Note that the heat transfer between the soil and the grout (14) is small due to the long characteristic time-scale of heat transport within the soil compared to that of the fluid flow. From Table 1, we note that actual Nusselt number ah/k_g between the soil and the grout is approximately $10^{-10}\approx\epsilon^2$. We define a scaled Nusselt number $Nu=L^2h/(ak_g)=O(1)$, which is unit-order compared to ϵ, as its multiple. Note that (9) can be obtained from (8) when $Pe=0$.

We approach the solution to this problem using a regular perturbation expansion (see [12]) in powers of the small aspect ratio ϵ for the “on” case (8). Using the expansion $T^{(1)}=T_0^{(1)}+\epsilon T_1^{(1)}+\cdots$ and introducing a second time-scale $\tau=\epsilon t$,

$$\begin{aligned}0=&\frac{1}{r}\frac{\partial}{\partial r}\left(r\frac{\partial T_0^{(1)}}{\partial r}\right)\\&+\epsilon\left\{\frac{1}{r}\frac{\partial}{\partial r}\left(r\frac{\partial T_1^{(1)}}{\partial r}\right)-\left(\frac{\partial T_0^{(1)}}{\partial t}+Pe(1-r^2)\frac{\partial T_0^{(1)}}{\partial x}\right)\right\}\\&+\epsilon^2\left\{\frac{1}{r}\frac{\partial}{\partial r}\left(r\frac{\partial T_2^{(1)}}{\partial r}\right)+\frac{\partial^2T_0^{(1)}}{\partial x^2}-\left(\frac{\partial T_1^{(1)}}{\partial t}+\frac{\partial T_0^{(1)}}{\partial\tau}+Pe(1-r^2)\frac{\partial T_1^{(1)}}{\partial x}\right)\right\}\\&+\cdots\end{aligned} \tag{15}$$

Similarly for the grout temperature, $T^{(2)}=T_0^{(2)}+\epsilon T_1^{(2)}+\cdots$,

$$\begin{aligned}0=&\alpha\frac{1}{r}\frac{\partial}{\partial r}\left(r\frac{\partial T_0^{(2)}}{\partial r}\right)+\epsilon\left\{\alpha\frac{1}{r}\frac{\partial}{\partial r}\left(r\frac{\partial T_1^{(2)}}{\partial r}\right)-\frac{\partial T_0^{(2)}}{\partial t}\right\}\\&+\epsilon^2\left\{\alpha\frac{1}{r}\frac{\partial}{\partial r}\left(r\frac{\partial T_2^{(2)}}{\partial r}\right)+\frac{\partial^2T_0^{(2)}}{\partial x^2}-\left(\frac{\partial T_1^{(2)}}{\partial t}+\frac{\partial T_0^{(2)}}{\partial\tau}\right)\right\}+\cdots\end{aligned} \tag{16}$$

From the $O(1)$ terms and using the boundary condition (12), it follows that $T_0^{(1)}$ and $T_0^{(2)}$ are independent of r, so they can be denoted by $T_0^{(1)}(x,t,\tau)=T_0^{(2)}(x,t,\tau)=\theta_0(x,t,\tau)$. This solution is in the nullspace of the operator $\partial_r(r\partial_r)$, and it corresponds to the portion of the solution with zero radial heat flux. This mode is always present at each stage of the analysis, and to close the problem mathematically, we assume that θ_o corresponds to the grout temperature at all orders in ϵ.

At $O(\epsilon)$, we find the following problem to solve for $T_1^{(1)},T_1^{(2)}$:

$$\frac{1}{r}\frac{\partial}{\partial r}\left(r\frac{\partial T_1^{(1)}}{\partial r}\right)=\left(\frac{\partial\theta_0}{\partial t}+Pe(1-r^2)\frac{\partial\theta_0}{\partial x}\right),\quad 0<r<1, \tag{17}$$

$$\frac{\alpha}{r}\frac{\partial}{\partial r}\left\{r\frac{\partial T_1^{(2)}}{\partial r}\right\}=\frac{\partial\theta_o}{\partial t},\quad 1<r<R, \tag{18}$$

subject to the boundary conditions

$$r\frac{\partial T_1^{(1)}}{\partial r}\to0\quad\text{as } r\to0, \tag{19}$$

$$\frac{\partial T_1^{(1)}}{\partial r}=k\frac{\partial T_1^{(2)}}{\partial r}\quad\text{at } r=1, \tag{20}$$

$$T_1^{(1)}=T_1^{(2)}\quad\text{at } r=1, \tag{21}$$

$$\frac{\partial T_1^{(2)}}{\partial r}=0\quad\text{at } r=R. \tag{22}$$

Solving (17) using (19) results in the solution for the first-order temperature correction, or the deviation of the fluid temperature from the local average temperature $\theta_o(x,t)$, is given by

$$T_1^{(1)}=\left\{\frac{r^2}{4}\left(\frac{\partial\theta_0}{\partial t}+Pe\frac{\partial\theta_0}{\partial x}\right)-Pe\frac{r^4}{16}\frac{\partial\theta_0}{\partial x}\right\}+\bar\theta_1^{(1)}(x,t,\tau). \tag{23}$$

Similarly for the deviation of the grout temperature from the local average temperature $\theta_o(x,t),T_1^{(2)}$, using (18) with (22) gives the following solution:

$$T_1^{(2)}=\frac{1}{\alpha}\frac{\partial\theta_0}{\partial t}\left(\frac{r^2}{4}-\frac{R^2}{2}\log r\right)+\bar\theta_1^{(2)}(x,t,\tau). \tag{24}$$

Applying the boundary condition (20) results in a compatibility condition for θ_o

$$\frac{\partial\theta_0}{\partial t}+v Pe\frac{\partial\theta_0}{\partial x}=0, \tag{25}$$

where

$$v=\frac{1}{2\left(1+\frac{k}{\alpha}[R^2-1]\right)}$$

is the speed at which leading-order temperature θ_o propagates in the axial direction *in the grout*. Note that this depends only on the material properties of the fluid and the grout, and relative cross-sectional areas of each. Thus θ_0 is constant along lines where $y=x-(vPe)t$ is constant, so that $\theta_0=\theta_0(y,\tau)$. Going back to find-

ing $T_1^{(1)}$ and $T_1^{(2)}$ from Eqs. (23) and (24) in this moving frame, we obtain

$$T_1^{(1)} = Pe\left\{(1-v)\frac{r^2}{4} - \frac{r^4}{16}\right\}\frac{\partial\theta_0}{\partial y} + \bar{\theta}_1^{(1)}(y,\tau), \tag{26}$$

$$T_1^{(2)} = v\frac{Pe}{\alpha}\left\{\frac{R^2}{2}\log r - \frac{r^2}{4}\right\}\frac{\partial\theta_0}{\partial y} + \bar{\theta}_1^{(2)}(y,\tau), \tag{27}$$

where we assumed that $\bar{\theta}_1^{(1)}(x,t,\tau) = \bar{\theta}_1^{(1)}(y,\tau)$ and $\bar{\theta}_1^{(2)}(x,t,\tau) = \bar{\theta}_1^{(2)}(y,\tau)$. Since we defined θ_o as the magnitude of the zero-radial-flux mode in the grout layer, $\bar{\theta}_1^{(2)} = 0$, and using (14) to equate temperatures at $r = 1$, we find that

$$\bar{\theta}_1^{(1)} = -\frac{Pe}{4\alpha}\left\{v(1-\alpha) + \frac{3\alpha}{4}\right\}\frac{\partial\theta_o}{\partial y}.$$

Now, turning to the $O(\epsilon^2)$ terms in Eqs. (15) and (16),

$$\frac{1}{r}\frac{\partial}{\partial r}\left(r\frac{\partial T_2^{(1)}}{\partial r}\right) = -\frac{\partial^2\theta_0}{\partial y^2} + \left(\frac{\partial T_1^{(1)}}{\partial t} + \frac{\partial\theta_0}{\partial\tau} + Pe(1-r^2)\frac{\partial T_1^{(1)}}{\partial x}\right), \tag{28}$$

$$\frac{\alpha}{r}\frac{\partial}{\partial r}\left(r\frac{\partial T_2^{(2)}}{\partial r}\right) = -\alpha\frac{\partial^2\theta_0}{\partial y^2} + \left(\frac{\partial T_1^{(2)}}{\partial t} + \frac{\partial\theta_0}{\partial\tau}\right). \tag{29}$$

The details of this analysis can be found in the Appendix A. To connect this result to observations, we convert back to the (x,t) framework (letting $\theta = \theta_o$ for notational convenience) and our equation for the averaged local temperature in the liquid and soil when the thermostat is on is given by

$$\theta_t + v\,Pe\,\theta_x = \epsilon(D\theta_{xx} - H\theta). \tag{30}$$

Note that the diffusion coefficient D and the effective heat transfer coefficient H are given by

$$D = D_F + D_T Pe^2, \tag{31}$$

$$H = \frac{2k\,Nu}{1 + \frac{k}{\alpha}(R^2-1)}, \tag{32}$$

where D_F is the Fourier diffusion component and D_T is the component due to Taylor dispersion.

The effect of the "off" cycle of the thermostat is that there is no fluid flow when the system does not demand power, and hence $Pe = 0$. Further, we assume that no axial heat flux moves to or from the system at $x = 0$, and we let $\theta_x = 0$ along $x = 0$ when the system is off. In summary, the unsteady problem under consideration can be written as"on":

$$\theta_t + Pe\,v\theta_x = \epsilon[D\theta_{xx} - H\theta], \tag{33}$$

$$x = 0: \quad \theta = 1, \tag{34}$$

$$x \to \infty: \quad \theta = 0, \tag{35}$$

"off"

$$\theta_t = \epsilon[D_F\theta_{xx} - H\theta], \tag{36}$$

$$x = 0: \quad \theta_x = 0, \tag{37}$$

$$x \to \infty: \quad \theta = 0. \tag{38}$$

We consider a time-harmonic solution to this problem, where P is the period of oscillation, and the cycle rate of the thermostat is given by η, or the percentage of time that the system is on. Both P and η are measures of the energy efficiency of the residence.

3. Results

3.1. Steady operation Pe≠0

As an introduction into the unsteady axial temperature variations from this model, we consider the problem (33) with boundary conditions (34) and (35). If we assume that the temperature has achieved a steady-state solution, then we can write (33) as an ordinary differential equation in x

$$\epsilon[D\theta_{xx} - H\theta] - v\,Pe\,\theta_x = 0. \tag{39}$$

The solution to (39) is of the form $\theta = A\exp(\sigma x)$, where σ is the spatial growth rate of the temperature. From the characteristic equation of (39), θ has two spatial exponential growth rates $\sigma_\pm$ defined as

$$\sigma_\pm = \frac{v\,Pe}{2\epsilon D}\left\{1 \pm \sqrt{1 + \frac{4\epsilon^2 DH}{(v\,Pe)^2}}\right\}. \tag{40}$$

By (35), the component with the positive growth rate σ_+ must be zero, which dictates that the only growth rate of interest is given by σ_-.

From (40), we can define the characteristic length $\ell_s = -1/\sigma_-$ as

$$\ell_s = \frac{v\,Pe}{2\epsilon H}\left\{\sqrt{1 + \frac{4\epsilon^2 HD}{v^2 Pe^2}} + 1\right\}. \tag{41}$$

Note that this length scale increases linearly with Pe as $Pe \to \infty$. To test this theory, we implement a numerical simulation of (33) with (34) and (35) over a domain scaled with $v\,Pe$. With this scaling, the discretization matrices of the terms in (33) are well conditioned, and a standard Crank–Nicolson scheme is used (see [13]). Fig. 2 shows the evolution of the time simulation for the parameter values $R = 5, Pe = 28,000$. The solid (blue) curve corresponds to the predicted exponentially decaying steady-state solution given by (40). Note that the temperature front propagates more slowly as time progresses, and the temperature behind the front converges to the expected steady-state value. We have also plotted the corresponding temperature disturbances from θ, T_1, in the (x,r) domain. Notice that there is a local hot spot (yellow/light) in the correction in the fluid and a corresponding cool spot in the grout layer that propagates with the temperature front, where the gradient of θ is maximum.

The front speed of this solution can be understood directly in terms of a similarity variable. The transformation

$$y = x - v\,Pe\,t \quad \theta = e^{-\epsilon Ht} f(y,t)$$

applied to (33) results in the standard heat equation for f:

$$f_t = \epsilon D f_{yy}.$$

The heat equation exhibits similarity solutions in terms of the similarity variable $\xi = y/(2\sqrt{\epsilon Dt})$. The location of this leading temperature change along the pipe in x corresponds to a fixed location in ξ. Thus the leading front $x_f(t)$ can be written as

$$x_f(t) = 2\xi\sqrt{\epsilon Dt} + v\,Pe\,t. \tag{42}$$

We compare (42) with the front speed of the decaying solution from our simulation over a range of Pe and R in Fig. 3. In all of these simulations, we normalized the data based on the final data value at $t = 5$. For each data point, 10 different simulations were taken with $3500 < Pe < 35,000$. The similarity values are all within 10^{-7} of the mean value. However, as R is increased, the solution converges more quickly to the similarity solution. This is consistent with $\alpha > 1$ based on the values used in Table 1. From this, we conclude that (42) characterizes the propagation of the front.

3.2. Unsteady flows

In residential applications, the fluid flows in the system in discrete stages. The cycling occurs on the advection time-scale (minutes) but we are interested in the temperature distribution on the conduction time scale (hours to days). To understand the unsteady behavior of (33)–(38), we can apply the technique of

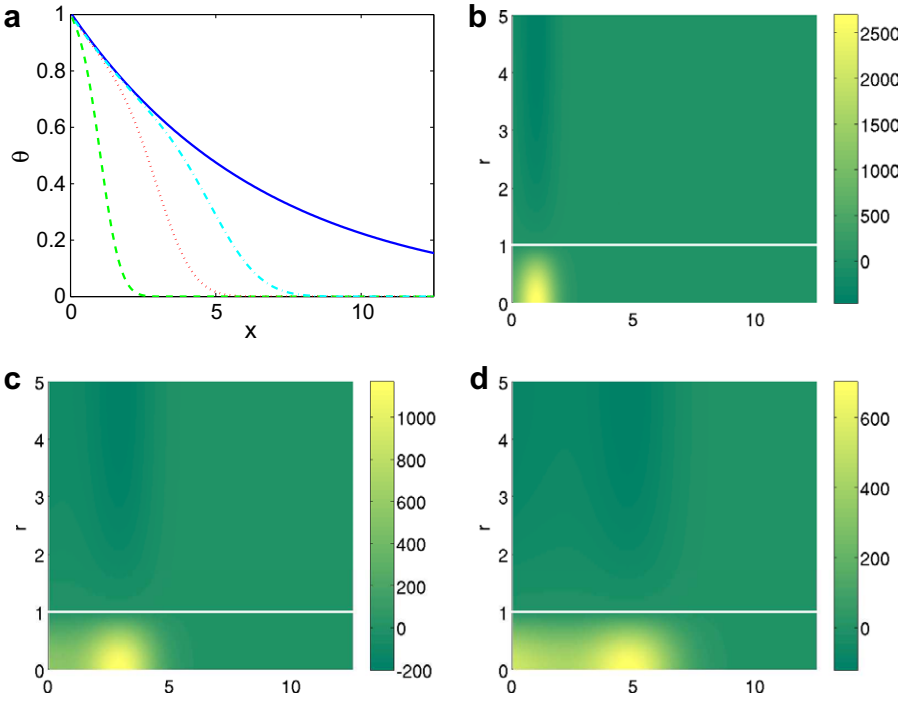

Fig. 2. (a) Snapshot of the temperature profiles for short times ($t = 1$ corresponds to nearly 27 h) from initial conditions of $\theta(x, 0) = 0$. The solid (blue) line corresponds to the steady-state temperature profile, the dashed (green) line corresponds to $t = 1$, the dotted (red) curve corresponds to $t = 3$, and the dashed-dot (cyan) curve corresponds to $t = 5$. Here $R = 5$ and $Pe = 28,000$. (b) The contour plot of the temperature correction T_1 over the axial and radial interval for $t = 1$. (c) $t = 3$, and $t = 5$. Note that the axial coordinate in figures (b)–(d) are in units scaled on υPe, which are significantly longer than the units for the radial dimension. (For interpretation of color mentioned in this figure legend the reader is referred to the web version of the article.)

homogenization in the limit of $P \to 0$. An example of this technique for microwave heating of laminates can be found in [14]. We define a second time-scale $t_p = O(1/\delta), \delta = P \ll 1$ on which θ is periodic, and assume that $\theta = \theta(x, t, t_p)$ where t, t_p are independent variables. Note that

$$\theta_t = \theta_t + \frac{1}{\delta}\theta_{t_p}.$$

For simplicity, assume that $\hat{\theta}$ represents a Fourier mode of the solution θ on $-\infty < x < \infty$. Note that since the system (33)–(38) is a linear system, an appropriate linear combination of these Fourier modes can be found that corresponds to the solution θ. In Fourier space, the problem can be written as

$$\hat{\theta}_{t_p} = -\delta\Big\{\hat{\theta}_t + \{\kappa^2\epsilon D + i\kappa\upsilon Pe + \epsilon H\}\hat{\theta}(t)\Big\}, \quad 0 < t_p < \eta, \tag{43}$$

$$\hat{\theta}_{t_p} = -\delta\Big\{\hat{\theta}_t + \{\kappa^2\epsilon D_F + H\}\hat{\theta}\Big\}, \quad \eta < t_p < 1, \tag{44}$$

where κ is the wavenumber of the temperature distribution θ.

Suppose that $\hat{\theta}(t_p = 0) = \hat{\theta}_o$. Then the solution to (43) is given by

$$\hat{\theta} = \hat{\theta}_o + \delta t_p\Big[\hat{\theta}_t + \{\kappa^2\epsilon D + i\kappa\upsilon Pe + \epsilon H\}\hat{\theta}\Big], \tag{45}$$

and similarly for $\eta < t_p < 1$,

$$\hat{\theta} = \hat{\theta}_o - \delta(t_p - \eta)\Big[\theta_t + \big[\kappa^2\epsilon D + \epsilon H\big]\hat{\theta}\Big] - \delta\eta\Big[\hat{\theta}_t + \{\kappa^2\epsilon D + i\kappa\upsilon Pe + \epsilon H\}\hat{\theta}\Big]. \tag{46}$$

Since we have defined θ to be periodic on the time-scale t_p, this gives us a restriction on the evolution of θ on the longer time-scale t:

$$\hat{\theta}_t = -\big[(\eta)\big[\kappa^2\epsilon D + i\kappa\upsilon Pe + \epsilon H\big] + (1-\eta)\big[\kappa^2\epsilon D_F\big] + \epsilon H\big]\hat{\theta}, \tag{47}$$

which can be represented in physical space as

$$\theta_t + \eta\upsilon Pe\,\theta_x = \epsilon[\eta D + (1-\eta)D_F]\theta_{xx} - \epsilon H\theta. \tag{48}$$

Note that the form of (48) is exactly the same as that found in (33). Hence, we can find the characteristic length scale for the unsteady case as

$$\ell_u = \frac{\upsilon Pe}{2\epsilon H}\left\{\eta + \sqrt{\eta^2 + \frac{4\epsilon^2 H D_{eff}}{(\upsilon Pe)^2}}\right\}, \tag{49}$$

where $D_{eff} = \eta D + (1-\eta)D_F$. Thus, in order to minimize the length of tubing required for the residential geothermal heating system to function, the heat losses of the residence need to be minimized.

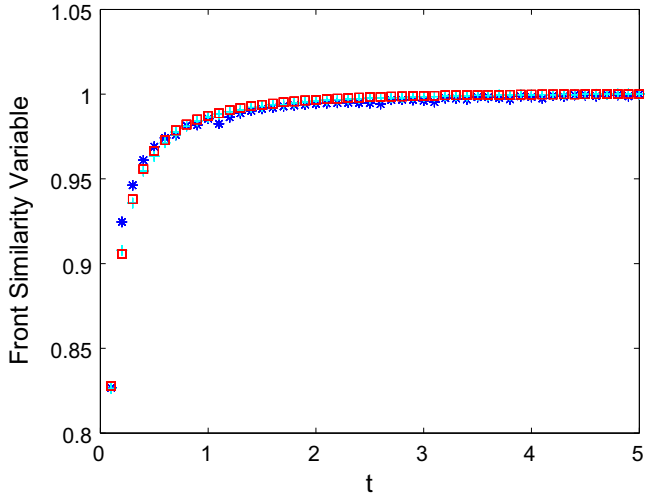

Fig. 3. Plot of simulation data in the similarity for from (42) for $3500 < Pe < 35,000$, and different radius ratios (10 simulations, each with a different Pe, per point). The points correspond to $R = 2$ (asterisk), $R = 4$ (crosses), $R = 6$ (squares). Notice that as R increases, the front converges more quickly to the similarity solution.

One way to measure this length is with respect to the steady characteristic length ℓ_s. If we consider their ratio

$$\frac{\ell_u}{\ell_s} = \frac{\eta v Pe + \sqrt{(v\eta Pe)^2 + 4\epsilon^2 H D_{eff}}}{v Pe + \sqrt{(v Pe)^2 + 4\epsilon^2 H D}} \sim \eta \quad \text{for } Pe \gg 1, \tag{50}$$

we note that the characteristic unsteady axial length scale depends linearly on the cycle rate of the system for large Peclet numbers. Further, the limit $\eta \to 0$ results in a value which is nonzero. While this latter result shows that there needs to be a lower bound for the length of the tubing in order for the system to be functional, it is not helpful to answer design questions. The effect of the unsteady flow is shown in Fig. 4, where analogous snapshots of the temperature profiles from Fig. 2 are displayed with $\eta = 1/2$ and $P = 0.01$. Note that the length x over which the temperature front propogates scales on η when compared to the steady case in Fig. 2.

Finally, we consider the similarity form of the unsteady equation (48) with the computational solution of (33)–(38). Fig. 5 shows the evolution of the front similarity variable for $\eta = 1/8$, $\eta = 1/4$, and $\eta = 1/2$ for $R = 2$. In the limit of small cycle rates, the effective similarity variable formulation for (48) better represents the evolution of (33)–(38).

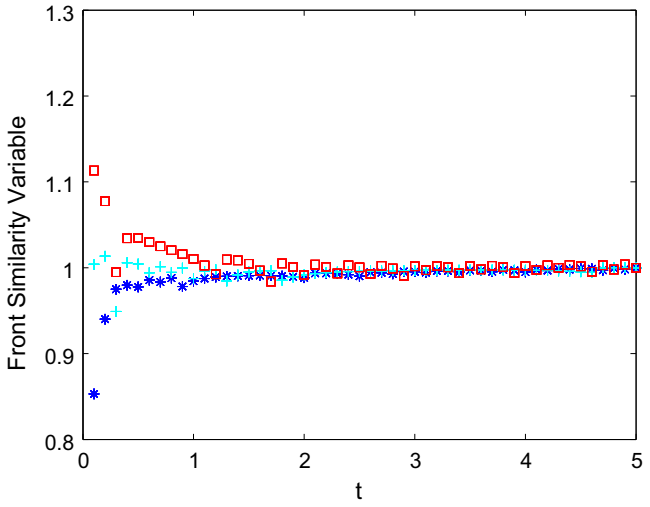

Fig. 5. Plot of simulated data of (33)–(38) with $P = 0.01$, and $\eta = 1/8$ (red square), $\eta = 1/4$ (cyan cross), and $\eta = 1/2$ (blue asterix). A minimum of 10 time steps were used for the smallest value of η, and each point corresponds to 10 different Pe, as in Fig. 3.

4. Conclusions

In this work, we describe the temperature profiles within a thin-walled tubing of a geothermal heat pump surrounded by a model soil. We find that the axial dispersion of the heat is significant under normal operating conditions, with the effective dispersion coefficient increasing with increasing flow rates. This physical effect in the cylindrical source model, has been modeled phenomenologically in the past, in addition to an additional thermal resistance effect separating the local and far-field thermal behavior in the soil. Our physically fundamental approach for this form of axial dispersion appears not to have been addressed in the ground source heat pump literature, and it appears to be a critical parameter in the optimization of these systems. The qualitative nature of our preliminary results for fluid/grout/soil systems are consistent with what is found here, but a more quantitative comparison of different materials using this model will be addressed in a later work.

We also have found that similarity solutions exist for steady flow, which is not a surprising result. However, under unsteady flow conditions, we find that the evolution of the front appears to be described in terms of this similarity variable. The propagation speed of the front is well described by the effective thermal front

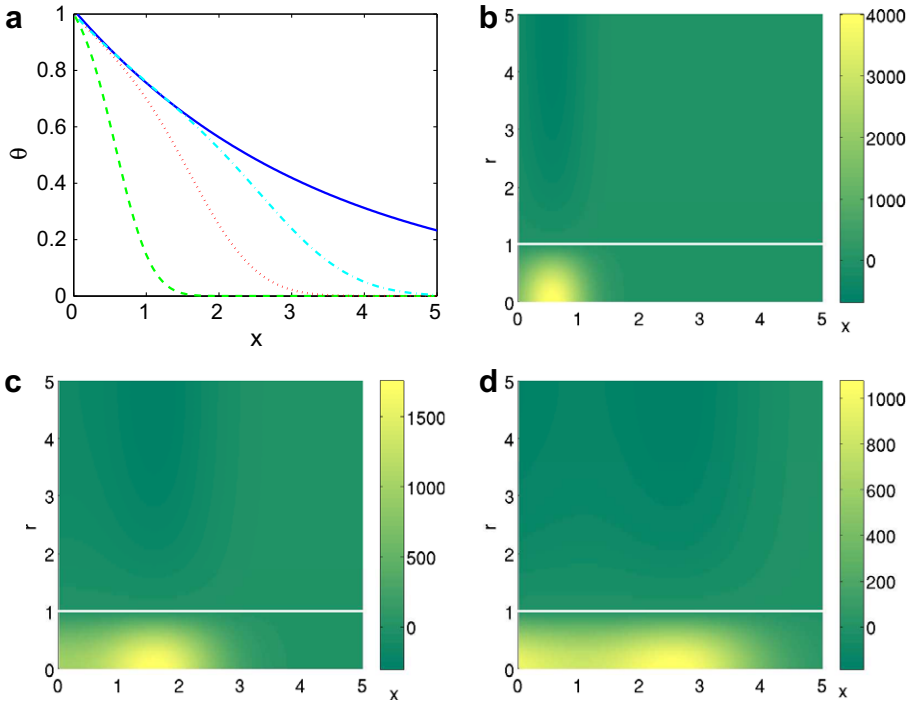

Fig. 4. (a) Snapshot of the unsteady temperature profiles for short times taken over the advective time-scale. The parameters and notation is the same as in Fig. 2, but here $\eta = 1/2$ and $P = 0.01$, which dimensionally corresponds to an on cycle of about 8 min. Note that the axial coordinate in figures (b)–(d) are in units of vPe, which are significantly longer than the units for the radial dimension.

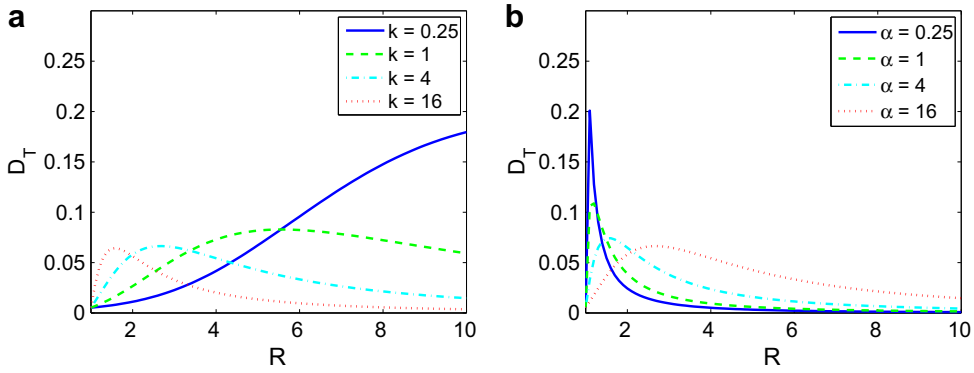

Fig. 6. (a) Taylor dispersion coefficient D_T as a function of borehole radius R for different values of thermal conductivity ratios k with $\alpha = 16$. (b) Taylor dispersion coefficient D_T as a function of R for different values of thermal diffusivities α with $k = 8$.

velocity and the Peclet number. This description may be sufficient to help in optimizing the design.

One additional insight from this analysis is how the effective length of tubing needed for normal operation of the system depends linearly on the efficiency (measured in terms of the cycle time per period between cycles) of the residence for large Peclet numbers. This appears not to have been considered in previous studies of these systems, but we recommend manufacturers of these systems to perform an energy audit of the residence before recommending any particular system to consumers.

From this analysis, the effect of Taylor dispersion acts to *extend* the required length of pipe for any given heat exchanger. Eq. (41) gives exactly the length when advection is balanced by radial heat transport in the limit when $D \to 0$. This effect persists when the flow is unsteady (see Eq. (49)). Hence, a design goal needed to minimize the required length resides in minimizing the Taylor dispersion portion of D. From Appendix A, this quantity depends only on R, k, and α.

Fig. 6 shows the dependence of the Taylor dispersion coefficient over a range of thermal conductivity ratios k and thermal diffusivity ratios, and thermal mass ratios α. Fig. 6a shows how the Taylor dispersion coefficient D_T varies over borehole radius R, with $\alpha = 16$ and different values of k, while Fig. 6b shows D_T over R with $k = 8$ and different values of α. Note that all of these curves have a maximum for a particular borehole radius, where the length of the tubing needs to be largest. However, this result demonstrates that the size of the borehole can be made larger or smaller based on the material properties of the grout and heat exchange fluid used.

Finally, we note that the current model is limited by the assumption of an ambient temperature in the soil in the far-field. This assumption is not valid during the seasonal changes that are typically found, nor on the time-scales when thermal depletion of the surrounding environment can take place. However, we note that from the local solution, we have an inner solution in the radial direction which describes the axial dependence of the radial heat flux as a function of r. This behavior can then be used in a matched asymptotic setting with the solution to the outer problem far from the borehole to form an effective evolution equation for the local temperature in the grout θ. We perform this extension of our analysis in an upcoming work [12]. The coupling of the local and far-field behavior for this simple annular geometry will allow us to mathematically model different geometries, and to understand the conditions under which different systems could yield better performance with lower installation costs.

Acknowledgement

A.O., V.Q.-B., and B.S.T. would like to thank Rensselaer's Graduate Student Mathematical Modeling Camp, funded by the National Science Foundation through Grant No. DMS-0308571. J.T. would like to thank the Olin College Faculty Research Program for their support.

Appendix A

Substituting $T_1^{(1)}$ and $T_1^{(2)}$ from Eqs. (26) and (27), and integrating over their respective radial domains, we find the radial temperature gradient at $r = 1$ from the fluid and the grout layer to be

$$\left(r\frac{\partial T_2^{(1)}}{\partial r}\right)\Big|_{r=1} = \frac{1}{2}\frac{\partial \theta_o}{\partial \tau} - \frac{1}{2}\frac{\partial^2 \theta_o}{\partial y^2} - \frac{Pe^2}{2} \times \frac{\partial^2 \theta_o}{\partial y^2}\left\{\frac{1}{192} + \frac{11\alpha+24}{48\alpha}\left(\frac{1}{2}-v\right) + \frac{7\alpha-1}{8\alpha}\left(\frac{1}{2}-v\right)^2\right\}, \tag{51}$$

$$\left(\frac{\partial T_2^{(2)}}{\partial r}\right)\Big|_{r=1} = \frac{R^2-1}{2}\frac{\partial^2 \theta_o}{\partial y^2} - \frac{1}{\alpha}\left(\frac{R^2-1}{2}\right)\frac{\partial \theta_o}{\partial \tau} + \frac{v^2 Pe^2}{2\alpha^2}\left[\frac{R^2-1}{2}\right]\left[\frac{R^4 \log R}{R^2-1} - \frac{3R^2+1}{4}\right] - Nu\,\theta_o. \tag{52}$$

Equating the heat flux across $r = 1$ gives us a compatibility equation for the mode amplitude θ_o:

$$\left[1 + \frac{k}{\alpha}(R^2-1)\right]\frac{\partial \theta_o}{\partial \tau} = [1 + k(R^2-1)]\frac{\partial^2 \theta_o}{\partial y^2} + Pe^2\left\{\frac{1}{192} + \left(\frac{11\alpha+24}{48\alpha}\right)\left(\frac{1}{2}-v\right) + \left(\frac{7\alpha-1}{8\alpha}\right)\left(\frac{1}{2}-v\right)^2\right\}\frac{\partial^2 \theta_o}{\partial y^2} \tag{53}$$

$$+ \frac{k v^2 Pe^2}{\alpha^2}\left[\frac{R^2-1}{2}\right]\left\{\frac{R^4 \log R}{R^2-1} - \frac{3R^2+1}{4}\right\}\frac{\partial^2 \theta_o}{\partial y^2} - \frac{2kNu}{Pe}\theta_o. \tag{54}$$

We can write this as $\theta_{o\tau} = D\theta_{oyy} - H\theta_o$, where D is the effective diffusivity of the medium, H the effective heat transfer coefficient. These can be written as

$$D = D_F + (D_{Tf} + D_{Tg})Pe^2, \tag{55}$$

$$D_F = \frac{1 + k[R^2-1]}{1 + \frac{k}{\alpha}[R^2-1]}, \tag{56}$$

$$D_{Tf} = \frac{1}{1 + \frac{k}{\alpha}[R^2-1]}\left\{\frac{1}{192} + \left(\frac{11\alpha+24}{48\alpha}\right)\left(\frac{1}{2}-v\right) + \left(\frac{7\alpha-1}{8\alpha}\right)\left(\frac{1}{2}-v\right)^2\right\}, \tag{57}$$

$$D_{Tg} = \frac{1}{1 + \frac{k}{\alpha}[R^2-1]}\frac{k v^2}{\alpha^2}\left[\frac{R^2-1}{2}\right]\left\{\frac{R^4 \log R}{R^2-1} - \frac{3R^2+1}{4}\right\}, \tag{58}$$

$$H=\frac{2kNu}{\left[1+\frac{k}{\alpha}(R^2-1)\right]}. \tag{59}$$

Note that the diffusion coefficient D has two components. The first component D_F corresponds to classical diffusion (Fourier's law), which decreases relative to the second component as the Peclet number increases. Previous analyses of typical geothermal heating systems neglect this term compared to the heat transfer from the grout layer to the surrounding soil. However, the second term of D is proportional to the square of the Peclet number, and corresponds to Taylor dispersion, and cannot be neglected for large Pe found in application. There are two components to this term, D_{Tf}, which corresponds to Taylor dispersion within the fluid, and D_{Tg}, which corresponds to Taylor dispersion between the fluid and the grout layer. Note that if the grout layer has zero thickness ($R \to 1$), then the Taylor dispersion term from this layer vanishes, and the Taylor dispersion term from the fluid reverts to the classical Taylor result (since $\upsilon \to 1/2$ in this limit).

References

[1] L. Ingersoll, O. Zobel, A. Ingersoll, Heat Conduction with Engineering Geological and Other Applications, second ed., McGraw-Hill, New York, 1954.

[2] H.S. Carslaw, J.C. Jaeger, Conduction of Heat in Solids, second ed., Oxford University Press, Oxford, 1959.

[3] L. Lamarche, B. Beauchamp, New solutions for the short-time analysis of geothermal vertical boreholes, Int. J. Heat Mass Transfer 50 (2007) 1408–1419.

[4] ASME International Solar Energy Conference, A modified analytical method for simulating cyclic operation of vertical U-tube ground-coupled heat pumps, 1995.

[5] C. Yavuzturk, J.D. Spitler, A short time step response factor model for vertical ground loop heat exchangers, ASHRAE Trans.: Research, 1999, pp. 475–485.

[6] M.G. Sutton, D.W. Nutter, R.J. Couvillion, R.K. Davis, An algorithm for approximating the performance of vertical bore heat exchangers installed in a stratified geological regime, ASHRAE Trans.: Research, 2002, pp. 177–194.

[7] M.K. Dobson, An experimental and analytical study of the transient behavior of verticle U-tube ground coupled heat pumps in the cooling mode, Master's Thesis, Texas A&M University, 1991.

[8] G.I. Taylor, Dispersion of soluble matter in solvent flowing slowly through a tube, Proc. Roy. Soc. London A 219 (1137) (1953) 186–203.

[9] G.I. Taylor, Conditions under which dispersion of a solute in a stream of solvent can be used to measure molecular diffusion, Proc. Roy. Soc. London A 225 (1163) (1954) 473–477.

[10] R. Aris, On the dispersion of a solute in a fluid flowing through a tube, Proc. Roy. Soc. London A 235 (1200) (1956) 67–77.

[11] A.J. Philippacopoulos, M.L. Berndt, Influence of debonding in ground heat exchangers used with geothermal heat pumps, Geothermics 30 (2001) 527–545.

[12] C.M. Bender, S.A. Orszag, Advanced Mathematical Methods for Scientists and Engineers, McGraw-Hill, New York, 1978.

[13] R.L. Burden, J.D. Faires, Numerical Analysis, sixth ed., Brooks/Cole, Belmont, CA, 1997.

[14] G.A. Kriegsmann, B.S. Tilley, Microwave heating of laminates, J. Eng. Math. 44 (2) (2002) 173–198.